KU LEUVEN

FACULTY OF SCIENCE
Department of Chemistry

Computational Exploration of Non-Valence Anions from Biological Quinones

A Second Order Approximate Coupled Clouster Study

DRAFT
To remove, add 'final' to class options

Mauro Gascón Navas

Dissertation presented in partial fulfillment
of the requirements for the degree of
Erasmus Mundus Master of Science in
Theoretical Chemistry and Computational
Modelling

Supervisors:
Robin Moorby
Prof. Dr. Thomas Jagau

June 2025

COMPUTATIONAL EXPLORATION OF NON-VALENCE ANIONS FROM BIOLOGICAL QUINONES

A SECOND ORDER APPROXIMATE COUPLED CLUSTER STUDY

Mauro GASCON NAVAS

Supervisors:
Robin Moorby
Prof. Dr. Thomas Jagau

Members of the
Examination Committee:
Prof. dr. ir. The Chairman, chair
Prof. dr. ir. The One
Prof. dr. ir. The Other
Prof. dr. External Jurymember
(Far Away)

Dissertation presented in partial fulfillment of the requirements for the degree of Erasmus Mundus Master of Science in Theoretical Chemistry and Computational Modelling

June 2025

© 2025 Mauro Gascón Navas
Uitgegeven in eigen beheer, Mauro Gascón Navas, Leuven (Belgium)

Alle rechten voorbehouden. Niets uit deze uitgave mag worden vermenigvuldigd en/of openbaar gemaakt worden door middel van druk, fotokopie, microfilm, elektronisch of op welke andere wijze ook zonder voorafgaande schriftelijke toestemming van de uitgever.

All rights reserved. No part of the publication may be reproduced in any form by print, photoprint, microfilm, electronic or any other means without written permission from the publisher.

Acknowledgements

. . .

Thank you thank you.

Instructions by the Arenberg Doctoral School:

The scientific abstract should present the most important aims and conclusions of the dissertation in a brief text of ca. 2 pages.

Abstract

...

Instructions by the Arenberg Doctoral School:

The scientific abstract should present the most important aims and conclusions of the dissertation in a brief text of ca. 2 pages.

Beknopte samenvatting

. . . aaa

Instructions by the Arenberg Doctoral School:

The scientific abstract should present the most important aims and conclusions of the dissertation in a brief text of ca. 2 pages.

List of Abbreviations

. 4

Contents

List of Figures

List of Tables

Chapter 1

Introduction

This chapter presents an overview of non-valence anions, focusing on dipole-bound anions (DBAs). The significance of these anions in biological systems is explored, followed by an introduction to biological quinones and their crucial role in biological processes. Finally, the research objectives are outlined.

1.1 Non-Valence Anions

An anion is an atom or molecule possessing one or more excess electrons. The binding of an additional electron to a neutral molecule is a balance between the attractive potential between the excess electron and the nuclei, and the repulsive forces from the neutral molecule's electrons. Unlike valence electrons in neutral species, these "extra" electrons do not experience a -1/r Coulombic attraction at long distances. Instead, they interact through weaker charge-multipole potentials, which are less robust than the covalent bonds holding the molecule together [1, 2].

The binding energy of the excess electron is typically significantly lower than the ionisation energy of the neutral molecule, leading to changes ranging from geometry relaxation to chemical reactions with surrounding species. In discussions of molecular anions, the concept of electron affinity (EA) is key. The adiabatic electron affinity (AEA) quantifies the energy difference between a molecule and its corresponding anion, both in their electronic ground states and lowest rovibrational levels. The vertical electron affinity (VEA), defined at the neutral equilibrium geometry, is particularly relevant for electron capture

dynamics. A molecule with a positive EA is considered electronically stable, requiring energy input to remove an electron from the anionic state [1].

Molecular anions are classified into valence anions, where the excess electron occupies a compact orbital similar to valence molecular orbitals, and non-valence anions (NVA) , where the excess electron occupies a diffuse orbital spatially separated from the molecule. Non-valence anions are further categorised based on the predominant long-range interaction responsible for electron binding: dipole-bound states (DBS), quadrupole-bound states (QBS), and correlation-bound states (CBS). These classifications lack rigorous definitions, and an NVA is typically stabilised by a range of interactions [1, 2, 3, 4, 5]. Examples of different anion types are shown in Figure 1.1.

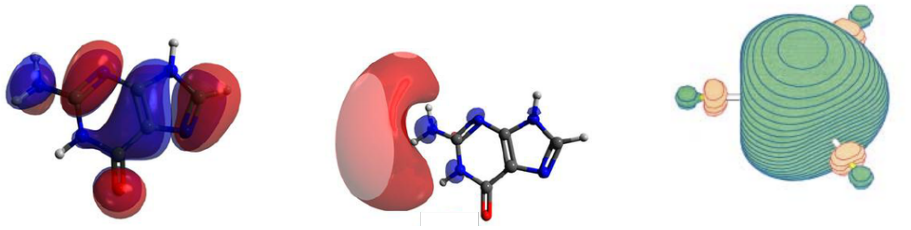

Valence anion *Dipole-bound anion* *$(HF)_3$ solvated electron*

Figure 1.1: Valence and Non-Valence Anions, a) and b) are reproduced from [6], c) from [5]. **I will substitute by my own figs**

1.1.1 Dipole-Bound Anions

Of the non-valence anions, dipole-bound anions (DBAs) are the most common and well-studied. Fermi and Teller first proposed the theoretical framework for non-valence bound states in 1947, demonstrating that a dipole could bind an excess electron if the dipole moment exceeds 1.625 D [7]. Further investigations refined this concept for "real" molecules, leading to a critical dipole moment of approximately 2.5 D [5].

The "weak" forces that bind the excess electron are responsible for the diffusive nature of the associated orbitals, often extending several Å from the neutral molecule, and their relatively low energy, usually below 0.1 eV. This makes them susceptible to external perturbations, such as solvent interactions or external electric fields, which can significantly influence their stability and reactivity [1, 2, 5].

Given that DBAs are bound with an energy comparable to thermal energy ($k_bT \sim 23$ meV), they may seem a theoretical curiosity with limited practical relevance, destined to undergo rapid autodetachment. However, some systems can undergo a nonadiabatic transition to a stable valence anion state [2, 5]. In this sense, DBSs act as "doorway" states for electron capture and transfer processes [8, 5, 9]. This behaviour has spurred interest in diverse fields from astrochemistry [10] to radiation biology [11, 12].

1.1.2 Approaches to Study Non-Valence Anions

Significant progress has been made in experimental and theoretical methodologies for elucidating the structure and dynamics of NVAs. Experimentally, dipole-bound anions are characterised using spectroscopic and mass spectrometric techniques designed to probe their weakly bound electronic states [1]. In photodetachment and photoelectron spectroscopies, a beam of anions is generated—often using a laser vaporisation or electrospray source—and intersected with a photon beam. The energy of the ejected electrons reveals information about the electron binding energy and electronic structure. Time-resolved photoelectron spectroscopy (TRPES) extends this approach, using ultrafast laser pulses to investigate the dynamics of electron attachment and detachment on femtosecond timescales, revealing transient states and relaxation pathways [13]. DBS can also be accessed by Rydberg electron transfer spectroscopy, which has been used to probe their role in electron transfer dynamics [14]. Time-of-flight mass spectrometry is often coupled with these techniques to identify and isolate the correct anionic species.

The theoretical investigation of DBAs presents two main challenges. Firstly, the large spatial extent of the DB orbital requires atomic orbital basis sets that are sufficiently diffuse to accurately describe it, necessitating the use of custom basis sets [15]. Secondly, electron correlation is important; although the electron in the DB orbital resides predominantly far from the precursor's valence electrons, the DB orbital is considerably polarisable due to its diffuse nature and exhibits significant dispersion-like interactions with the other valence electrons, contributing substantially to its binding energy [1, 4, 16].

Regarding computational methods, standard density functional theory (DFT) approaches can fail due to their inadequate treatment of the highly diffuse electron density and can suffer from spin contamination in open-shell systems, requiring careful selection of the exchange-correlation functional [17]. Multiconfigurational methods like complete active space self-consistent field (CASSCF) can address the multiconfigurational nature of these systems, but require considerable expertise in selecting an appropriate active space that

balances accuracy and computational feasibility. Currently, equation-of-motion coupled-cluster (EOM-CC) methods represent the standard for DBA modelling as they adequately capture both electron correlation effects and open-shell character. However, the high computational cost of EOM-CC approaches significantly limits their applicability to larger molecular systems [2, 5]. To address this, some approximate methods have been developed, such as the second order approximate CC [18]- which is used in this work, or the domain-based pair natural implementation (DLPNO) method [19].

1.1.3 Non-Valence Anions In Condensed Matter

Several studies have indicated that the presence of individual molecules interacting with a molecule supporting an NVA can further stabilise the state by strengthening the total dipole moment, or by combining individual moments to form a "cavity" where the electron resides. The excess electron is stabilised by the collective interaction with multiple solvent molecules, rather than binding to any individual molecule, and is known as a solvated electron [5, 2, 20, 21]. The binding energy of such solvated electrons can increase dramatically with cluster size; while a water dimer anion $(H_2O)_2^-$ exhibits a very weak vertical detachment energy (VDE) of only 0.045 eV, water cluster anions $(H_2O)_n^-$ with approximately 80–100 molecules can achieve VDEs exceeding 2.0 eV. A weakly bound non-valence state transforms into a strongly bound electronic species with significantly altered properties [2]. In bulk, the hydrated electron is bound at 2.2 eV [5, 22]. The structure of the state was subject of much debate in the literature [22, 5], but it is now generally accepted that the excess electron resides in a cavity of approximately 2.5 Å in size [22].

In solution, the existence of a hydrated DBA is still debated [23, 24]. The survival of NBS in condensed matter remains a subject of discussion. Computational studies suggest that hydration influences the localisation of the excess electron, often displacing it onto the solvent cage's surface [23]. Conversely, experimental evidence indicates that alkyl chains do not disrupt DBS stability [24], and DBS-mediated mechanisms have been observed in solvated uracil systems [25]. The viability of NBS in bulk systems depends on the molecular density and polarity of the medium. While solvents may hinder DBS existence due to excluded volume effects, they also stabilise DBS through Van der Waals interactions [14, 26]. Distinct scenarios can be considered in the interaction between a DBA supporting molecule and solvent: the electron may be localised in the NVA orbital, captured by the solvent to form a cage, or interact with solvent molecules whose instantaneous dipole orientations stabilise the DB state. The latter two phenomena are linked to charge-transfer-to-solvent (CTTS) electronic transitions and are observed experimentally [4, 14, 26].

1.1.4 Non-Valence Anions in Biological Systems

Expand this section explaining more about the DNA and radiosensitizers. End with some sentences about the experimants w quinones. Research on DBAs has predominantly focused on gas-phase systems. In biological contexts, DBAs have been studied for their interactions with DNA, particularly in radiation damage and radiosensitisation [27, 11, 12].

Studies on electron interactions with biomolecules, both in bare and hydrated states, have highlighted the significance of DBAs in biological systems. The role of NVAs in natural biological pathways outside genetic damage remains largely unexplored. Their sensitivity to environmental factors suggests potential applications in regulating long-range electron transfer processes. It has been suggested that in proteins, vacant pockets could accommodate non-valence states [24].
expand this section with electron transfer in proteins and more discussion? Most studies related to the biological importance of these NVAs are done in relation to DNA. In this study, we aim to focus on other biological targets, which could use an interplay between NVAs and valence bound electrons. A compound that is ubiquitous in nature and whose structure is interesting to study is ubiquinone.

1.2 Biological Quinones

Quinones, first isolated from the bark of the cinchona tree in the 18th century [28], are a class of organic compounds with a fully conjugated cyclic dione structure derived from aromatic compounds by conversion of an even number of C-H groups into carbonyl (ketone) C=O groups [29]. Quinones are known for their redox properties and play crucial roles in various biological processes, including electron transport in cellular respiration and photosynthesis [30, 31].

This work focuses on ubiquinone -*ubi* from being ubiquitous in nature-, also known as coenzyme Q_{10} (CoQ_{10}), a lipid-soluble molecule that exists as a quinone or quinol, then named ubiquinol. It plays a role in aerobic respiration in the electron transport chain (ETC) as an electron carrier, accepting 2 electrons at complexes I and II and donating them in complex III [30]. CoQ_{10}.

1.2.1 Structural Aspects of Ubiquinone

Ubiquinone is composed of a benzoquinone ring and a long isoprenoid side chain, which varies in length depending on the organism. The number of isprenoid units is the n in the Q_n scheme. The benzoquinone moiety is responsible for its redox properties, while the isoprenoid tail enhances its lipid solubility, allowing it to integrate into biological membranes [30]. The benzoquinone moiety consists of 2,3-dimethoxy-6-methyl-p-benzoquinone [30].

As stated, the quinone moiety is responsible for its electron binding properties; it supports two anion states, a valence anion and a dipole bound anion. The valence anion can be understood as the equivalent state to the parent molecule, p-benzoquinone, with the excess electron located in a π^* orbital. The electron withdrawing ketone groups contribute to stabilise this state, which is bound in the range of 1.7 eV [31]. The dipole-bound anion, on the other hand, results mainly from the two methoxy chains, whose configuration mainly controls the dipole of the molecule [32]. The interplay between these groups, especially in the case of Q_0 - without any isoprenoid molecule, makes it a very interesting system to study theoretically. It is a fairly rigid molecule, except for the dihedral angles between the methoxy groups and the benzoquinone ring, which can be used to control the dipole moment of the molecule. This makes the study of a fairly complicated electronic structure in terms of two coordinates.

When the isoprenoid tail is considered, it has been shown that it further stabilises the valence anion [33]. Regarding its effects on the dipole state, one can imagine the effect to be moderate; it will slightly modify the dipole moment of the system, but structurally it will be quite far from the orbital occupied by the

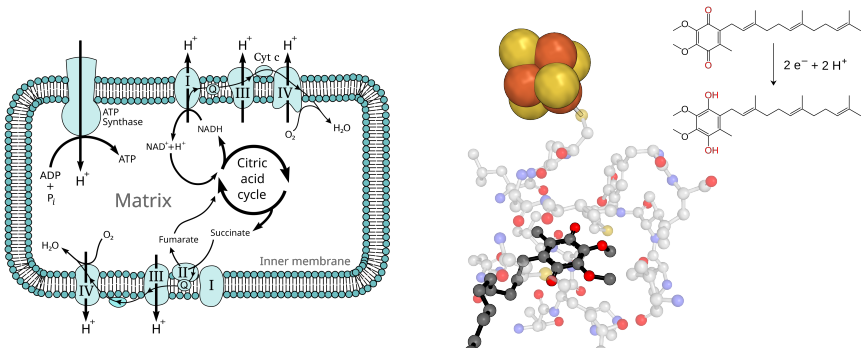

Figure 1.2: **Role of ubiquinone. I will fix later**

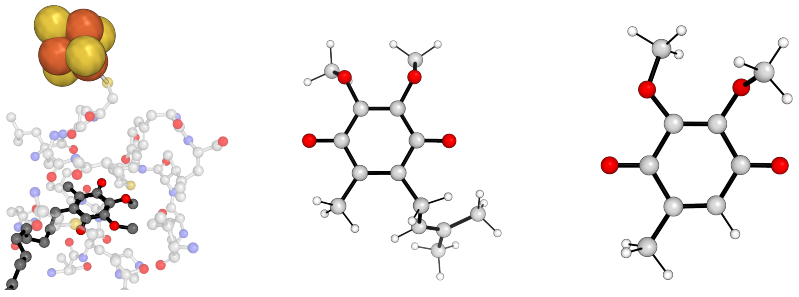

Q10, Cluster Model Q1 Q0

Figure 1.3: Quinones used in this work. From left to right: (a) Q_0, (b) Q_1, (c) Q_{10} in the enzyme PDB bla bla.

excess electron.

There have been extensive studies on the electron binding properties of the ubiquinone family, both experimentally [32, 34, 33, 35] and theoretically [32, 33, 19, 36, 37]. However, these studies have been centred on understanding the valence anion of the quinone, and no comprehensive study of its dipole bound state has been performed; the VBA is the final acceptor of the electron and the existence of the DBA in condensed phase is dubious. However, experimental studies have observed dipole-bound anions in the gas phase in ubiquinones Q_0 and Q_1 [32] with an EA of ∼60 meV. Although its signal is reduced as more isoprenoid units are added, interpreted as an effect of the isprenoid tail being flexible and resulting in a steric hindrance of the state [32, 33], one could imagine that in a protein moiety, the geometry of the tail would be fixed far from a potential DB orbital, which could even be further stabilised by residues pointing in the cavity.

1.3 Research Objectives

The main objective of this work is to study the dipole-bound anion of ubiquinone. The specific objectives are:

- Benchmark the effectiveness of the CC2 method to model quinones electron attachment.
- To investigate the dipole-bound anion of ubiquinone as a function of its methoxy groups, and the effect of the isoprenoid tail.

- To study the effect of the protein environment on the dipole-bound anion of ubiquinone, treated as a cluster model using small molecules.

Chapter 2

Theoretical Background

2.1 Self Consistent Field Methods

The objective of any quantum chemical calculation is to solve the time-independent Schrödinger equation (TISE) for a many-electron system:

$$\hat{H}\Psi = E\Psi \tag{2.1}$$

However, solving the TISE exactly for systems with more than one electron is computationally infeasible due to the complexity of electron-electron interactions. To address this, approximate methods such as the Hartree-Fock (HF) method have been developed[38].

The Hartree-Fock (HF) method stands as the cornestone electronic structure calculations. Its primary objective is to provide an approximate solution to the many-electron time-independent Schrödinger equation within the Born-Openhaimer approximation, which governs the behavior of electrons within atoms and molecules: The HF method achieves this by assuming that each electron moves independently within an average electrostatic field generated by the other electrons in the system. In the HF method the N-electron wavefunction is represented by a Slater determinant, which is formed by taking the antisymmetrized product of N individual one-electron spin-orbitals (χ):

$$\Psi(\mathbf{r}_1, \mathbf{r}_2, \ldots, \mathbf{r}_N) = \frac{1}{\sqrt{N!}} \begin{vmatrix} \chi_1(\mathbf{r}_1) & \chi_2(\mathbf{r}_1) & \cdots & \chi_N(\mathbf{r}_1) \\ \chi_1(\mathbf{r}_2) & \chi_2(\mathbf{r}_2) & \cdots & \chi_N(\mathbf{r}_2) \\ \vdots & \vdots & \ddots & \vdots \\ \chi_1(\mathbf{r}_N) & \chi_2(\mathbf{r}_N) & \cdots & \chi_N(\mathbf{r}_N) \end{vmatrix} \tag{2.2}$$

The choice of using a deteminant inherently satisfies both the Pauli exclusion principle, and the antisymmetry requirement of fermions. The energy expectation for a Slater determinant according to HF is variational and can be computed as:

$$\begin{aligned} E_{HF} &= \langle\Psi|\sum_{i=1}^{N}\hat{F}_i|\Psi\rangle \\ &= \langle\Psi|\sum_{i=1}^{N}\hat{h}(i) + \sum_{i,j=1}^{N}(2\hat{J}_j(i) - \hat{K}_j(i))|\Psi\rangle \\ &= \sum_{i=1}^{N}\langle\chi_i|\hat{h}|\chi_i\rangle + \frac{1}{2}\sum_{i,j=1}^{N}\langle\chi_i\chi_j||\chi_i\chi_j\rangle \end{aligned} \tag{2.3}$$

Where, $\hat{F}$ is the Fock operator. $\hat{F}$ is made up from $\hat{h}$, the one-electron core Hamiltonian operator (kinetic energy and electron-nucleus attraction); $\hat{J}_j(i)$, the Coulomb operator, describing the electrostatic repulsion between electron i and the average charge distribution of electron j, and $\hat{K}_j(i)$ is the exchange operator, a purely quantum mechanical term arising from the antisymmetry principle. Because of the two electron terms, the computational cost of HF scales as $O(N^4)$.

The Hartree-Fock equations are inherently non-linear: because the Fock operator depends on the wavefunctions of all the other electrons, their interactions are coupled. Consequently, these equations cannot be solved analytically and are solved using an iterative procedure known as the self-consistent field (SCF) method, where the final field experienced by the electrons must be consistent with the electron distribution that generates that field. The SCF procedure involves the following steps: An initial guess for the spin-orbitals is made. Using this initial guess, the Fock operator is constructed. The Hartree-Fock equations are then solved by diagonalizing the Fock operator to obtain a new set of molecular orbitals and their corresponding energies. This new set of orbitals is compared to the previous set. If the change is below a predefined threshold, the procedure is considered converged, and the SCF is achieved. If convergence is not reached, the new set of orbitals is used to construct a new Fock operator, and the process is repeated. Convergence signifies that a stable electronic configuration has been reached within the limitations of the Hartree-Fock approximation.

In practical Hartree-Fock calculations, the spinorbitals are expressed as linear combinations of predefined mathematical functions known as basis functions. The set of these functions is called a basis set. Because a finite basis set cannot exactly represent the spinorbitals, they greatly define the level of accuracy

and computational cost of the calculation. Larger basis sets generally lead to more accurate descriptions of the electronic structure at the cost of increased computational effort.

2.1.1 Electron Correlation

The Hartree-Fock (HF) method is inherently limited by its neglect of the instantaneous interactions of electrons. In the HF approximation, each electron is treated as moving independently within a static, average field created by the other electrons. This mean-field approach fails to account for the fact that electrons will instantaneously repel each other, leading to a correlated movements as they try to avoid each other in space.
The primary consequence of neglecting electron correlation in the HF approximation is an overestimation of the electron-electron repulsion energy. While the HF method does account for the exchange interaction exactly as a consequence of the antisymmetry of the Slater determinant (Fermi correlation), it completely neglects the Coulomb, or dynamic, correlation. This omission leads to a higher electronic energy than the exact solution, and an inability to accurately predict certain phenomena, such as London dispersion forces.
The difference between the exact non-relativistic energy of the system and the energy obtained in the HF complete basis limit is defined as the correlation energy and is always negative due to the variational principle. Correlated methods aim to include the effects of the instantaneous interactions between electrons that are neglected in the mean-field approximation of HF theory. In the following sections, several correlated methods relevant to this work are presented.

2.1.2 Møller-Plesset Perturbation Theory

Møller-Plesset (MP) perturbation theory offers a way to improve upon the HF energy by the use of Raylei-Schro perturbation theory: the electron correlation is treated as a perturbation to the HF Hamiltonian. The energy and wavefunction are then expanded as a series in terms of the perturbation strength. The first-order energy correction in MP theory is zero, so the first non-trivial correction to the HF energy appears at the second order, giving rise to the MP2 method. The MP2 energy correction for a closed-shell molecule is given by:

$$E_{\mathrm{MP2}} = -\frac{1}{4}\sum_{ij}^{\mathrm{occ}}\sum_{ab}^{\mathrm{virt}}\frac{|\langle ij||ab\rangle|^2}{\epsilon_a + \epsilon_b - \epsilon_i - \epsilon_j} \tag{2.4}$$

Where i, j denote occupied molecular orbitals, a, b denote virtual molecular orbitals, and ϵ are the corresponding orbital energies from the HF calculation. MP theory can be extended to higher orders (MP3, MP4, etc.) to achieve greater accuracy, although the computational cost increases significantly with each order. The computational cost of MP2 scales as $O(N^5)$.

2.1.3 Density Functional Theory

Density Functional Theory (DFT) provides an alternative approach to incorporating electron correlation by parametrizing the energy on the electron density rather than the wavefunction, reducing the degrees of freedom of the system from $3N - 3$ to just 3. In the most commonly used form of DFT, the Kohn-Sham method, the prpblem is formulated terms of orbitals that are not physical, but are chosen to reproduce the electron density of the system. The fundamental principle of DFT is that the ground state energy of a system is a unique functional of its electron density:

$$\left(-\frac{1}{2}\nabla^2 + \hat{V}_{\text{ext}}(\mathbf{r}) + \hat{V}_{\text{H}}(\mathbf{r}) + \hat{V}_{\text{XC}}[\rho(\mathbf{r})]\right)\psi_i(\mathbf{r}) = \epsilon_i\psi_i(\mathbf{r}) \tag{2.5}$$

Where $\hat{V}_{\text{ext}}$ respresents the external potential, $\hat{V}_{\text{H}}(\mathbf{r}) = \int \frac{\rho(\mathbf{r}')}{|\mathbf{r}-\mathbf{r}'|}d\mathbf{r}'$ is the Hartree potential, $\hat{V}_{\text{XC}}$ is the Exchange-Correlation potential and $\rho(\mathbf{r})$ is the electron density. The exchange-correlation functional is the most challenging part of DFT, as it is not known exactly and must be approximated. The accuracy of DFT calculations depends heavily on the choice of exchange-correlation functional. The computational cost of DFT scales as $O(N^4)$.

2.1.4 Configuration Interaction

Configuration Interaction (CI) methods improve upon HF by expressing the electronic wavefunction as a linear combination of the HF ground state determinant and excited state determinants:

$$|\Psi_{\text{CI}}\rangle = c_0|\Phi_0\rangle + \sum_{ia} c_{ia}|\Phi_{ia}\rangle + \sum_{ijab} c_{ijab}|\Phi_{ijab}\rangle + \dots \tag{2.6}$$

Where $|\Phi_0\rangle$ is the HF ground state determinant, $|\Phi_{ia}\rangle$ represents a determinant with a hole in spin-orbital i and a particle in the spin-orbital a, and c are the CI coefficients. Full CI (FCI), includes all possible excitations within a given one-electron basis set and represents the exact solution to the non-relativistic Schrödinger equation in that basis. However, is computationally prohibitive

for all but the simplest systems. Full Configuration Interaction (FCI) includes all possible excitations within a given one-electron basis set and represents the exact solution to the non-relativistic Schrödinger equation in that basis. However, it is computationally prohibitive for all but the simplest systems.
Truncated CI methods, such as CISD (singles and doubles), are more practical but lack size extensivity —a property ensuring that the energy of a system scales correctly with the number of non-interacting subsystems. A method is size-extensive if, for two infinitely separated molecules A and B, the total energy satisfies $E(A+B) = E(A) + E(B)$. Truncated CI methods fail to satisfy this condition because they do not include all necessary higher-order excitations, leading to an underestimation of the total energy as system size grows.
CI are, however, size-consistent, meaning that the energy behaviour remains consistent when interaction between the involved molecular subsystems is nullified (by distance, for instance). While CISD is size-consistent, its lack of size extensivity makes it unsuitable for extensive systems.

2.1.5 Coupled Cluster Theory

Similarly to CI, the coupled cluster CC method expands the wavefunction as a linear combination of Slater determinats. However, the CC wavefunction is size-extensive and size-consistent by using an exponential ansatz,

$$|\Psi_{\mathrm{CC}}\rangle = e^{\hat{T}}|\Psi_0\rangle \tag{2.7}$$

where $\hat{T}$ is the cluster operator, which is the central component of CC theory and is defined as a sum of excitation operators,

$$\hat{T} = \hat{T}_1 + \hat{T}_2 + \hat{T}_3 + \cdots + \hat{T}_N \tag{2.8}$$

where N is the total number of electrons in the system. Each term in this sum corresponds to a specific level of excitation and is expressed within the second quantization formalism:

- $\hat{T}_1 = \sum_i^{\mathrm{occ}} \sum_a^{\mathrm{virt}} t_i^a a_a^\dagger a_i$ represents single excitations.
- $\hat{T}_2 = \frac{1}{4} \sum_{i,j}^{\mathrm{occ}} \sum_{a,b}^{\mathrm{virt}} t_{ij}^{ab} a_a^\dagger a_b^\dagger a_j a_i$ represents double, *coupled* excitations.
- Higher-order excitation operators $\hat{T}_3, \hat{T}_4, \ldots$ describe coupled excitation of three, four, and more electrons, respectively.

The coefficients t_i^a, t_{ij}^{ab}, etc., are cluster amplitudes to determined by projection of the CC Schrödinger equation onto the excited determinant. The exponential

form, expanded as a Taylor series,

$$e^{\hat{T}} = 1 + \hat{T} + \frac{1}{2!}\hat{T}^2 + \dots \tag{2.9}$$

inherently includes terms that represent disconnected clusters, which are ensures for size consistency. The energy is obtained by projecting onto the HF reference determinant:

$$E_{\text{CC}} = \langle \Psi_0 | e^{-\hat{T}} \hat{H} e^{\hat{T}} | \Psi_0 \rangle \tag{2.10}$$

Using the Baker-Campbell-Hausdorff expansion, the exponential operators in Eq. 2.10 can be simplified to a series of commutators which ends at the fourth order. The cluster operator $\hat{T}$ can be truncated at different levels of excitation:

- **CCD** (Coupled Cluster Doubles): This is the simplest approximation in the CC family, where the cluster operator is truncated to include only double excitations: $\hat{T} \approx \hat{T}_2$. There is no CC Singles since the Brilluin's theorem implies that the amplitudes of single excitations alone are null.
- **CCSD** (Coupled Cluster Singles and Doubles): This is one of the most widely used and generally accurate *ab initio* methods, where the cluster operator includes both single and double excitations: $\hat{T} \approx \hat{T}_1 + \hat{T}_2$.
- **CCSDT** (Coupled Cluster Singles, Doubles, and Triples): $\hat{T} \approx \hat{T}_1 + \hat{T}_2 + \hat{T}_3$.
- ...

The hierarchy can be extended to include even higher levels of excitation, with the properties converging to the FCI limit. The computational cost of CC methods increases rapidly with the level of truncation, as shown in Table 2.1.

Method	Operation count	Memory
HF	$O(N^4)$	$O(N^4)$
DFT	$O(N^4)$	$O(N^4)$
MP2	$O(N^5)$	$O(N^4)$
CCD/CCSD	$O(N^6)$	$O(N^4)$
CCSDT	$O(N^8)$	$O(N^6)$
CC2	$O(N^5)$	$O(N^4)$

Table 2.1: Computational scaling of quantum chemistry methods.

2.1.6 Second Approximate Coupled Cluster

Second Approximate Coupled Cluster (CC2) belongs to the broader family of CCn approximate coupled cluster methods, where the 'n' in CCn indicates the truncation of the cluster operator within a perturbative hierarchy. These methods aim to reduce the computational cost associated with standard CC truncations while still retaining a reasonable level of accuracy.

In CC2, the equations for the single amplitudes, t_i^a, are the same as CC theory (Eq. 2.7) under the constraint that the doubles amplitudes, t_{ij}^{ab}, are calculated using the non-iterative expression for MP2 (Eq 2.4). The resulting expression for the CC2 correlation energy is:

$$E_{\mathrm{CC2}} = \frac{1}{4}\sum_{ij}^{\mathrm{occ}}\sum_{ab}^{\mathrm{virt}}\frac{|\langle ij||ab\rangle|^2}{\epsilon_a+\epsilon_b-\epsilon_i-\epsilon_j} + \sum_{i}^{\mathrm{occ}}\sum_{a}^{\mathrm{virt}}\hat{F}_{ai}t_i^a \tag{2.11}$$

The perturbative treatment of the doubles amplitudes in CC2, reduces the computational cost compared to CCSD, Table 2.1. While this approximation can lead to a less accurate description of electron correlation, the inclusion of singles amplitudes allows for an approximate description of orbital relaxation, which often leads to higher quality wavefunction, and hence properties, compared to MP2.

2.2 Equation-of-Motion Methods

Equation-of-Motion Coupled Cluster (EOM-CC) methods are an extension of ground-state coupled cluster theory which provide a framework for calculating a variety of excited (EE), ionized (IP) and electron-attached (EA) states. In the EOM-CC, the target electronic state is generated by applying a linear excitation operator $\hat{R}$ to a reference state, which typically is the coupled cluster wavefunction of the ground state. The target state wavefunction can then be expressed as $|\Psi_{\mathrm{EOM}}\rangle = \hat{R}|\Psi_{\mathrm{CC}}\rangle = \hat{R}e^{\hat{T}}|\Phi_{\mathrm{HF}}\rangle$. Figure 2.1, shows some of the determinats of $|\Psi_{\mathrm{EA}}\rangle$, where the target state has one more α electron.

The form of the operator $\hat{R}$ is similar to the cluster operator and chosen to access the desired target state. In the case of EOM-EA, the electron attachment operator R^{EA} includes terms that describe the creation of one electron to an unoccupied orbital, terms that describe the creation of one electron accompanied by the excitation of another electron from an occupied to an unoccupied orbital,

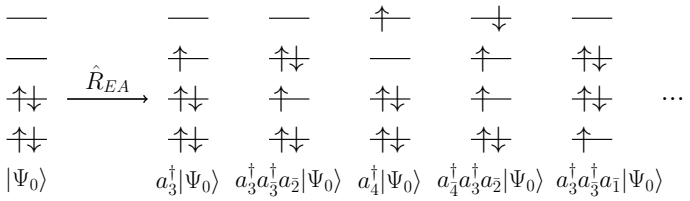

Figure 2.1: EOM-EA.

and so on:

$$\hat{R}^{\mathrm{EA}} = \hat{R}_1^{\mathrm{EA}} + \hat{R}_2^{\mathrm{EA}} + \ldots = \sum_a r^a a_a^\dagger + \frac{1}{2}\sum_{ab}\sum_i r_i^{ba} a_b^\dagger a_a^\dagger a_i + \ldots \tag{2.12}$$

Where a and b denote virtual orbitals, i denotes an occupied orbital, and r^a and r_i^{ba} are the coefficients to be determined. By truncating at the same excitation level as the cluster operator, the method is rigorously size-extensive and size-consistent. The EA energies, or any other EOM energy, can be obtained as the eigenvalues of the similarity-transformed Hamiltonian, $\bar{H}_{\mathrm{N}}$:

$$\bar{H}_{\mathrm{N}}\hat{R}|\Psi_0\rangle = \Delta E_{\mathrm{EOM}}\hat{R}|\Psi_0\rangle \tag{2.13}$$

$$\bar{H}_{\mathrm{N}} = e^{-\hat{T}}\hat{H}e^{\hat{T}} - \langle\Psi_0|e^{-\hat{T}}\hat{H}e^{\hat{T}}|\Psi_0\rangle \tag{2.14}$$

Since the similarity trnasformed hamiltonian is non-hermitian, the left and right are different but correspond to the same eigenvalues. This means that the properties have 'right' and 'left' expectation values.
The strength of the EOM-CC ansatz is the use of a closed shell reference to access open shell states, which are eigenfunctions of the $\hat{S}^2$ operator. The EOM-CC methods are also size-extensive and size-consistent. The computational cost of EOM-CC methods is similar to that of the corresponding ground-state CC methods.

2.3 Dyson Orbitals

Dyson orbitals are defined as the overlap between the wavefunction of an initial N-electron state ($|\Psi_0^N\rangle$) and the wavefunction of the final state with $N \pm 1$ electrons ($|\Psi_f^{N\pm1}\rangle$).

$$\phi_d(r_1) = \sqrt{N}\int \Psi^N(r_2,\ldots,r_N)\Psi^{N+1}(r_1,r_2,\ldots,r_N)\,dr_2\ldots dr_N \tag{2.15}$$

Because the the terms differ in one electron, the result of the overlap is a vector instead of a scalar, and can be expressed as a linear combination of the molecular orbitals ($\phi_p(r)$) of the reference wavefunction:

$$\phi_d(r) = \sum_p \gamma_p \phi_p(r) \tag{2.16}$$

where γ_p are the coefficients that quantify the contribution of each molecular orbital to the Dyson orbital. Physically, Dyson orbitals can be interpreted as the correlated analog to the orbital of the electron that is either removed or attached.

The norm squared of the Dyson orbital, (P), is calculated by integrating the squared modulus of the Dyson orbital over all space:

$$P = \int |\phi_{Dyson}(r)|^2 \, dr = \sum_{p,q} \gamma_p^* \gamma_q \langle \phi_p | \phi_q \rangle \tag{2.17}$$

The pole strength ranges from 0 to 1 and provides a direct measure of the one-electron character of the ionization or electron attachment process. As the open shell wavefunction is usually obtained by means of a EOM-CC method, there are a 'left' and 'right' Dyson orbital.

They can be used for the interpretation and prediction of photoelectron spectra as they contain all the information required to calculate diffrential corss-sections, $\frac{d\sigma}{d\Omega_k}$:

$$\frac{d\sigma}{d\Omega_k} = \frac{4\pi^2 k E}{c} |\langle \phi_d | \mu | \Psi_k^{el} \rangle|^2 \tag{2.18}$$

where where k is the magnitude of the photoelectron wavevector, E is the energy of the ionizing radiation, and c is the speed of light, μ is the dipole operator, and Ψ_k^{el} is the photoelectron wavefunction, and a strong orthonormality is assumed between the reference and continuum wavefunction.

2.3.1 EOM-CC2 Dyson Orbital Equations

Justify that the expression doesnt change from CCSD (see TJ email).

EOM-EA-Dyson Equations

A derivation of the algebraic expression of Dyson orbitals in terms of the t, r, l, λ amplitudes is presented. It is importnat to realize that the operators

involved ($\hat{T}, \hat{\Lambda}, \hat{R}, \hat{L}$) affect the occupation of the spin-orbitals, and thus only the combinations of terms which leave the refrence wavefunction, $|0\rangle$, unchanged survive. To find these combinations, commutators can be used to reorder the operators involved:

In the case of the right EOM-EA-Dyson orbital amplitudes:

$$\gamma_i^{\mathrm{EA,R}} = \langle EA|\hat{a}_i^\dagger|CC\rangle = \langle 0|\hat{L}^{EA}e^{-\hat{T}}\hat{a}_i^\dagger e^{\hat{T}}|0\rangle$$

The following equalities are usueful:

$$e^{-\hat{T}}e^{\hat{T}} = e^{\hat{T}}e^{-\hat{T}} = 1$$

$$[e^{\pm\hat{T}}, \hat{a}_p^\dagger] = \cancelto{0}{[1, \hat{p}^\dagger]} \pm t_j^b[\hat{b}^\dagger\hat{j}, \hat{p}^\dagger] \pm t_{jk}^{bc}[\hat{b}^\dagger\hat{c}^\dagger\hat{k}\hat{j}, \hat{p}^\dagger] + \dots$$

Where a change of notation, $a_p^\dagger \to p^\dagger$, upon expansion is done for readibility. Two cases are distinguished, p is a virtual orbital, a, or an occupied orbital, i. For virtual orbitals, $p = a$:

$$[\hat{b}^\dagger\hat{j}, \hat{a}^\dagger] = \hat{b}^\dagger\hat{j}\hat{a}^\dagger - \hat{a}^\dagger\hat{b}^\dagger\hat{j} = (-1)^2\hat{a}^\dagger\hat{b}^\dagger\hat{j} - \hat{a}^\dagger\hat{b}^\dagger\hat{j} = 0$$

Similarly with higher order terms, it is arribed to:

$$[e^{\pm\hat{T}}, \hat{a}_a^\dagger] = 0$$

For occupied orbitals, $p = i$:

$$[\hat{b}^\dagger\hat{j}, \hat{\imath}^\dagger] = \hat{b}^\dagger\hat{j}\cancelto{0}{\hat{\imath}^\dagger} - \hat{\imath}^\dagger\hat{b}^\dagger\hat{j}$$

And similarly with higher order terms:

$$[e^{\pm\hat{T}}, \hat{a}_i^\dagger] = -\hat{a}_i^\dagger(e^{\pm\hat{T}} - 1)$$

These relations can now be used to derive the expression for the occupied and virtual Right EOM-EA-Dyson orbital amplitudes:

$$\phi_{\mathrm{D}}^{\mathrm{EA,R}} = \sum_p \gamma_p^{\mathrm{EA,R}}\phi_p = \sum_i^{\mathrm{occ}} \gamma_i^{\mathrm{EA,R}}\phi_i + \sum_a^{\mathrm{vir}} \gamma_a^{\mathrm{EA,R}}\phi_a$$

The general expression can be reordered:

$$\begin{aligned}\gamma_p^{\mathrm{EA,R}} &= \langle EA|\hat{a}_p^\dagger|CC\rangle = \langle 0|\hat{L}^{EA}e^{-\hat{T}}\hat{a}_p^\dagger e^{\hat{T}}|0\rangle \\ &= \langle 0|\hat{L}^{EA}(\hat{a}_p^\dagger e^{-\hat{T}} + [e^{-\hat{T}}, \hat{a}_p^\dagger])e^{\hat{T}}|0\rangle \end{aligned} \tag{2.19}$$

For virtual orbitals, $p = a$:

$$\begin{aligned}
\gamma_a^{\mathrm{EA,R}} &= \langle 0|\hat{L}^{EA}(\hat{a}_a^\dagger e^{-\hat{T}} + \cancelto{0}{[e^{-\hat{T}}, \hat{a}_a^\dagger]})e^{\hat{T}}|0\rangle \\
&= \langle 0|\hat{L}^{EA}\hat{a}_a^\dagger \cancel{e^{-\hat{T}}e^{\hat{T}}}^{1}|0\rangle = \langle 0|\hat{L}^{EA}\hat{a}_a^\dagger|0\rangle \\
&= \langle 0|l_a \hat{a}\hat{a}^\dagger|0\rangle \\
&= l_a
\end{aligned} \tag{2.20}$$

For occupied orbitals, $p = i$:

$$\begin{aligned}
\gamma_i^{\mathrm{EA,R}} &= \langle 0|\hat{L}^{EA}(\hat{a}_i^\dagger e^{-\hat{T}} + [e^{-\hat{T}}, \hat{a}_i^\dagger])e^{\hat{T}}|0\rangle \\
&= \langle 0|\hat{L}^{EA}(\cancelto{0}{\hat{a}_i^\dagger e^{-\hat{T}} - \hat{a}_i^\dagger e^{-\hat{T}}} + \hat{a}^\dagger)e^{\hat{T}}|0\rangle = \langle 0|\hat{L}^{EA}\hat{a}_i^\dagger e^{\hat{T}}|0\rangle \\
&= \langle 0|l_b t_i^b\, \hat{b}\hat{i}^\dagger\hat{b}^\dagger\hat{i} + l_{bc}^j t_{ij}^{bc}\, \hat{b}\hat{c}\hat{j}^\dagger\hat{i}^\dagger\hat{b}^\dagger\hat{c}^\dagger\hat{i}\hat{j}|0\rangle \\
&= -\sum_c t_{ic} l_c - \frac{1}{2}\sum_{kcd} t_{ki}^{dc} l_{dc}^k
\end{aligned} \tag{2.21}$$

A similar approach can be applyed to the other Dyson equations to obtain the expressions.

Left EOM-EA-Dyson orbital, $\phi_{\mathrm{D}}^{\mathrm{EA,L}} = \sum_i^{\mathrm{occ}} \gamma_i^{\mathrm{EA,L}}\phi_i + \sum_a^{\mathrm{vir}} \gamma_a^{\mathrm{EA,L}}\phi_a$:

$$\begin{aligned}
\gamma_i^{\mathrm{EA,L}} &= \langle CC|\hat{a}_i|EA\rangle \\
&= -\sum_c \lambda_{ic} r_c - \frac{1}{2}\sum_{kcd} \lambda_{ik}^{cd} r_k^{dc}
\end{aligned} \tag{2.22}$$

$$\begin{aligned}
\gamma_a^{\mathrm{EA,L}} &= \langle CC|\hat{a}_a|EA\rangle \\
&= r_a + \sum_{kc} \lambda_{kc} r_{ca}^k + \sum_k \gamma_k^{\mathrm{EA,L}} t_{ka} - \frac{1}{2}\sum_{klcd} \lambda_{lk}^{dc} t_{lk}^{da} r_c
\end{aligned} \tag{2.23}$$

EOM-EA-EE-Dyson Equations

Right Dyson orbital, $\phi_{\mathrm{D}}^{\mathrm{EA-EE,R}} = \sum_i^{\mathrm{occ}} \gamma_i^{\mathrm{EA-EE,R}}\phi_i + \sum_a^{\mathrm{vir}} \gamma_a^{\mathrm{EA-EE,R}}\phi_a$:

$$\gamma_i^{\mathrm{EA-EE,R}} = \langle EA|\hat{a}_i^\dagger|EE\rangle$$

$$= r_0\gamma_a^{\mathrm{EA,R}} - \sum_c r_{ic}l_c - \frac{1}{2}\sum_{lcd} r_{il}^{cd}l_{dc}^{l} - \sum_{lcd} l_{dc}^{l}t_{ic}r_{ld} \tag{2.24}$$

$$\gamma_a^{\mathrm{EE-EA,R}} = \langle EA|\hat{a}_a^\dagger|EE\rangle$$

$$= r_0 l_a + \sum_{kc} l_{ca}^{k}r_{kc} \tag{2.25}$$

Left Dyson orbital, $\phi_{\mathrm{D}}^{\mathrm{EE-EA,L}} = \sum_i^{\mathrm{occ}} \gamma_i^{\mathrm{EE-EA,L}}\phi_i + \sum_a^{\mathrm{vir}} \gamma_a^{\mathrm{EE-EA,L}}\phi_a$:

$$\gamma_i^{\mathrm{EE-EA,L}} = \langle EE|\hat{a}_i|EA\rangle$$

$$= -\sum_c l_{ic}r_c - \frac{1}{2}\sum_{kcd} l_{ik}^{cd}r_k^{dc} \tag{2.26}$$

$$\gamma_a^{\mathrm{EE-EA,L}} = \langle EE|\hat{a}_a|EA\rangle$$

$$= \sum_{kc} l_{kc}r_{ca}^{k} + \sum_k \gamma_k^{\mathrm{EE-EA,L}}t_{ka} - \frac{1}{2}\sum_{klcd} l_{lk}^{dc}t_{lk}^{da}r_c \tag{2.27}$$

EOM-IP-Dyson Equations

Right Dyson orbital, $\phi_{\mathrm{D}}^{\mathrm{EE,R}} = \sum_i^{\mathrm{occ}} \gamma_i^{\mathrm{IP,R}}\phi_i + \sum_a^{\mathrm{vir}} \gamma_a^{\mathrm{IP,R}}\phi_a$:

$$\gamma_a^{\mathrm{IP,R}} = \langle CC|\hat{a}_a^\dagger|IP\rangle$$

$$= \lambda_{ka}r_k + \frac{1}{2}\lambda_{lk}^{ca}r_{klc} \tag{2.28}$$

$$\gamma_i^{\mathrm{IP,R}} = \langle CC|\hat{a}_i^\dagger|IP\rangle$$

$$= r_i + \sum_{kc} \lambda_{kc}r_{ik}^{c} - \sum_c \gamma_c^{\mathrm{IP,R}}t_{ic} - \frac{1}{2}\sum_{klcd} \lambda_{lk}^{dc}t_{li}^{dc}r_k \tag{2.29}$$

Left Dyson orbital, $\phi_{\mathrm{D}}^{\mathrm{IP,L}} = \sum_i^{\mathrm{occ}} \gamma_i^{\mathrm{IP,L}} \phi_i + \sum_a^{\mathrm{vir}} \gamma_a^{\mathrm{IP,L}} \phi_a$:

$$\begin{aligned}\gamma_i^{\mathrm{IP,L}} &= \langle IP|\hat{a}_i|CC\rangle \\ &= l_i \end{aligned} \tag{2.30}$$

$$\begin{aligned}\gamma_a^{\mathrm{IP,L}} &= \langle IP|\hat{a}_a|CC\rangle \\ &= \sum_k t_{ka} l_k + \frac{1}{2}\sum_{klc} t_{kl}^{ac} l_{kl}^{c} \end{aligned} \tag{2.31}$$

EOM-EE-IP-Dyson Equations

Right Dyson orbital, $\phi_{\mathrm{D}}^{\mathrm{EE-IP,R}} = \sum_i^{\mathrm{occ}} \gamma_i^{\mathrm{EE-IP,R}} \phi_i + \sum_a^{\mathrm{vir}} \gamma_a^{\mathrm{EE-IP,R}} \phi_a$:

$$\begin{aligned}\gamma_i^{\mathrm{EE-IP,R}} &= \langle EE|\hat{a}_i^\dagger|IP\rangle \\ &= \sum_{kc} l_{kc} r_{ik}^{c} - \sum_c \gamma_c^{IP-EI} t_{ic} - \frac{1}{2}\sum_{klcd} l_{lk}^{dc} t_{li}^{dc} r_k \end{aligned} \tag{2.32}$$

$$\begin{aligned}\gamma_a^{\mathrm{EE-IP,R}} &= \langle EE|\hat{a}_a^\dagger|IP\rangle \\ &= l_{ka} r_k + \frac{1}{2} l_{lk}^{ca} r_{klc} \end{aligned} \tag{2.33}$$

Left Dyson orbital, $\phi_{\mathrm{D}}^{\mathrm{IP-EE,L}} = \sum_i^{\mathrm{occ}} \gamma_i^{\mathrm{IP-EE,L}} \phi_i + \sum_a^{\mathrm{vir}} \gamma_a^{\mathrm{IP-EE,L}} \phi_a$:

$$\begin{aligned}\gamma_i^{\mathrm{IP-EE,L}} &= \langle IP|\hat{a}_i|EE\rangle \\ &= r_0 l_i + \sum_{kc} l_{ik}^{c} r_{kc} \end{aligned} \tag{2.34}$$

$$\begin{aligned}\gamma_a^{\mathrm{IP-EE,L}} &= \langle IP|\hat{a}_a|EE\rangle \\ &= r_0 \gamma_a^{\mathrm{IP,L}} + \sum_k r_{ka} l_k + \frac{1}{2}\sum_{klc} r_{kl}^{ac} l_{kl}^{c} + \sum_{klc} l_{kl}^{c} t_{ka} r_{cl} \end{aligned} \tag{2.35}$$

Chapter 3

Computational Methods

All electronic structure calculations were performed using the developer's copy of the *Q-Chem* software [39]. In all computations the frozen-core approximation is used, only the valence electrons are correlated, as well as the resolution of the identity (RI) approximation, auxiliary basis functions are used to approximate the two-electron integrals, reducing its scaling to $N(O^3)$ [40].

For the EOM-EA calculations, the reference wavefunction was obtained as the restricted Hartree-Fock (RHF) solution of the ground state of the neutral molecule. Unless explecitly mentioned, calculations were performed at using the aug-cc-pVDZ basis set [41] further augmented by 3 s-shells on hydrogen atoms and 6 s- and 3 p-shells on all non-hydrogen atoms [42] to properly model the non-valence states. The coefficients of the extra functions were obtained by successively halving the most diffuse function of the original set.

CC2 Dyson obitals for EOM variants described in section 2.3.1 and appendix **??** were implemented as described, and will be released in an upcoming verion of *Q-Chem*.

All closed-shell quinone model geometries were optimized using the TPSS functional[43] with Grimme's pair-wise dispersion corrections with Becke-Johnson damping (D3BJ)[44], and the minimally augmented[45] def2-TZVP basis sets[46] (ma-def2-TZVP), following the work in [47]. For the scan calculations, each singlepoint was optimized constraining its relevant angles by the method of Lagrange multipliers; dihedrals of the methoxy chains of Q0 and Q1,and the isoprene tail of Q1. In the case of quinone + aminoacid models, crystal structures were taken from the Protein Data Bank (PDB). Hydrogens were added using *PyMOL*'s [48] `add_H` functionality, and relaxed using the

method above (fixing the rest of the heavy atoms).

For the scans of quinone + molecule, each subsystem was independently optimized and and put together with any further refinement.

For quinone stystems, only EOM-EA right Dyson orbitals were computed to speed up the calculations by avoiding the need to compute the lamda terms.

Photoionization and Photodetachment crossections were calculated using the *ezDyson* package [49, 50].

Chapter 4

Results and Discussion

4.1 Performance of EOM-CC2 Related Methods

...

4.1.1 Basis Set Dependence of EA-EOM-CC2 in Dipole Bound Anions

...

		RI-CC2						RI-CCSD			
			aug-cc-pVTZ			pVDZ	pVQZ	pVDZ	pTDZ		
Molecule		2s1p	4s2p	6s3p	8s4p	6s3p	6s3p	6s3p	6s3p	KT	μ(D)
Acetaldehyde	CH_3CHO	-156.7	-27.8	-3.2	0.8	-4.6	-3.2	-4.6	-3.1	-0.4	3.29
Acetone	$(CH_3)_2CO$	-114.9	-16.8	1.3	3.3	-0.3	0.9	-0.5	0.9	-5.1	3.46
Acetonitrile	CH_3CN	-61.2	12.6	19.9	20.1	18.2	20.3	17.1	18.4	4.2	4.29
Benzaldehyde	C_6H_5CHO	-97.1	-2.1	8.9	9.6	7.4	9.1	3.4	4.6	-4.9	3.77
N,N-Dimethylformamide	$(CH_3)_2NCHO$	-81.1	5.4	14.1	14.4	13.2	14.4	13.3	13.7	1.9	4.48
DMSO	$(CH_3)_2SO$	-84.5	4.0	15.4	16.1	14.8	15.5	14.7	14.9	2.1	4.63
Formamide	CH_3NO	-92.2	1.1	16.2	17.2	15.1	17.0	15.1	15.9	3.4	4.28
Methylisocyanide	CH_3NC	-95.1	-0.5	10.0	10.5	9.5	10.1	8.8	9.0	-1.8	3.59
Nitrobenzene	$C_6H_5NO_2$	-63.6	30.6	34.8	34.8	32.5	-	25.0	25.9	5.4	5.15
Nitromethane	CH_3NO_2	-82.9	5.7	14.2	14.7	13.0	14.7	12.9	13.7	3.5	4.10
Nitrosobenzene	C_6H_5NO	-125.0	1.0	11.4	-	9.9	-	5.1	6.0	-4.1	3.73
Phenylisocyanide	C_6H_5NC	-82.7	8.6	16.3	16.5	15.2	16.7	9.0	9.2	-4.9	3.61
Pyridazine	$C_4H_4N_2$	-80.7	20.5	26.3	26.4	25.0	26.7	18.6	19.1	1.7	4.41
Vinylene carbonate	$C_3H_2O_3$	-82.5	20.9	27.2	27.4	26.4	27.7	25.1	25.5	10	5.05
	MAE	105.3	8.8	2.8	3.4	2.3	2.4	0.8	ref.	12.0	

Table 4.1: EOM-EA binding energies of dipole-bound radical anions computed using different augmented Dunning basis sets and RI-CC2 and RI-CCSD for the the test set of moluces [42]. A positive value corresponds to a bound electron. Koopmans' theorem (KT), and dipole momment (μ), calculated at the HF level, and mean absolute error (MAE) are also given. The values are in meV and D respectively.

4.1.2 Performance of EA-EOM-CC2 on Valence Bound Radical Anion States of Quinones

Mol.	Ref. [47]		RI-CC2	
	Exp (aEA)	CCSD(T) $+E_{CBS}$	No SCS	SCS
1	1.91	1.64	2.02	1.54
2	1.85	1.57	1.95	-
3	1.76	1.49	1.89	1.39
4	1.77	1.5	1.89	1.40
5	1.69	1.43	1.84	1.34
6	1.62	1.42	1.83	1.32
7	1.72	1.32	1.65	1.17
8	1.86	1.5	1.88	1.39
9	1.81	1.55	1.97	-
10	1.74	1.51	1.92	1.45

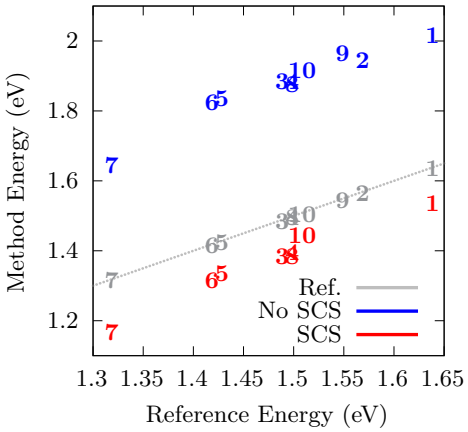

Table 4.2 and **Figure 4.1:** Comparison between reference and RI-CC2 data for quinones. The table also includes the experimental value (adiabatic EA instead of veritacl EA).

SCS improves the result for valence state of CC2, whihc is in accordance with the conclusions from [42]. Something to note is that when comparing the results with experiments, one can think that CC2 gets close than CCSD. This however, can be explained by the fact that the experiment measures the adiabatic electron binding energy, while the calculations are performed for the vertical EA. As the former energy

As the trend is recovered without SCS, albeit the larger (0.2 eV) but consist error the subsequent calculations do not use this method, as SCS worsens the results for dipole bound anions. A strength of this approach is that both states can be calculated from the same Hamiltonian, and the results are consitent.

Dipole bound states are worsen by SCS [42]. This is explaned by the fact that the DBS resides in a digguse state; the extra spin is far from the other electrons, meaning that the exchange interaction is much smaller than the Coulumb interaction. ...

4.1.3 Photoelectron Cross-section Calculations from EOM-CC2/CCSD

...

4.2 Study on the Anion States of Ubiquinone

...

4.2.1 Energy and Dipole Surfaces of CoQ

...

Q0

aa

...

Q1

...

...

4.2.2 Interaction with Water

...

4.2.3 Effect of Nearby Amionacids

...

Serine

...

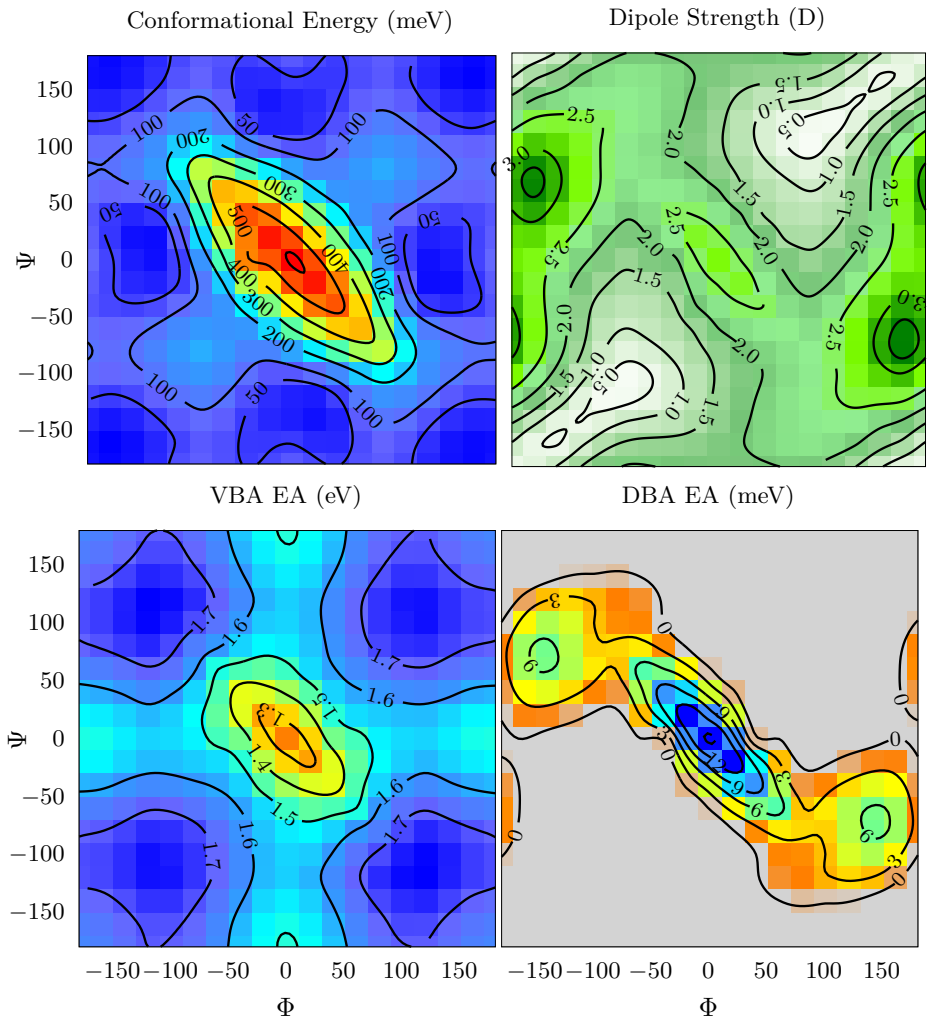

Figure 4.2: Surfaces of Q0. Left: Energy surface. Right: Dipole moment surface.

Threonine

...

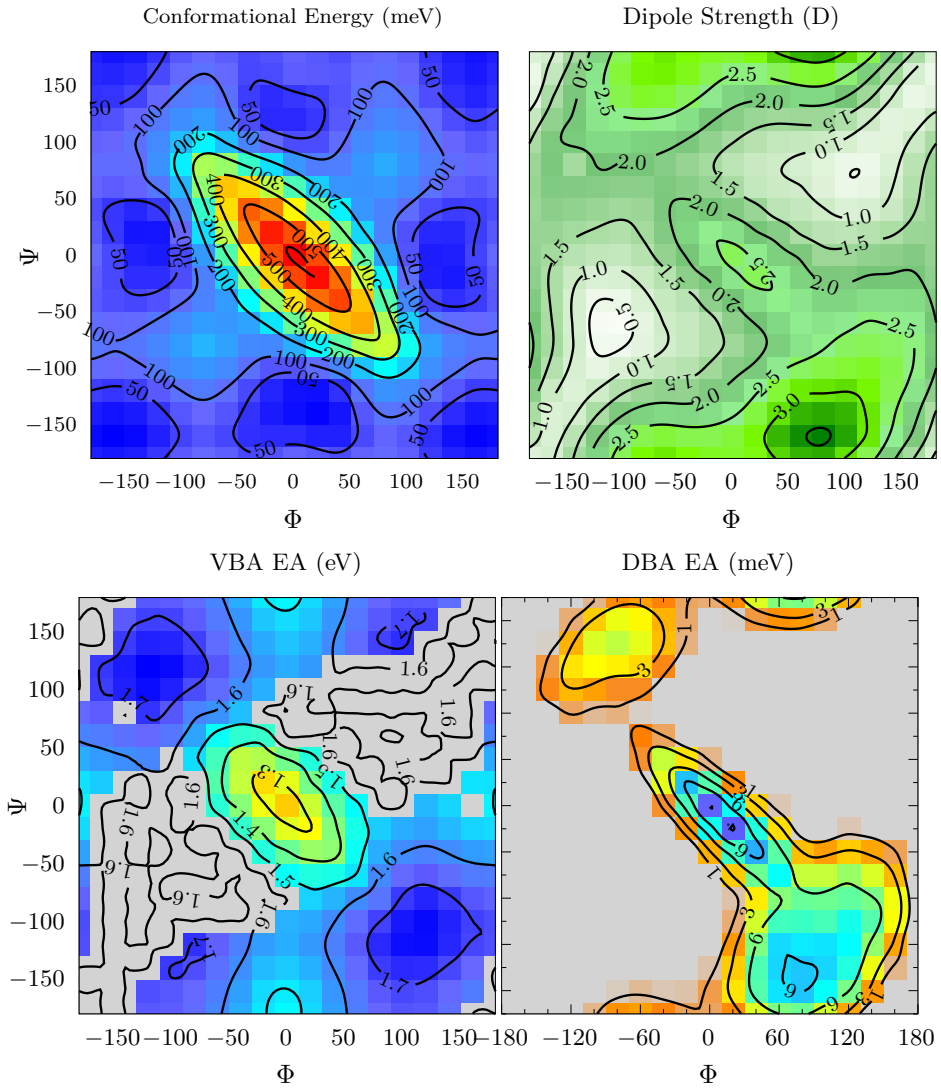

Figure 4.3: Surfaces of Q1. Left: Energy surface. Right: Dipole moment surface.

Apsaragine

...

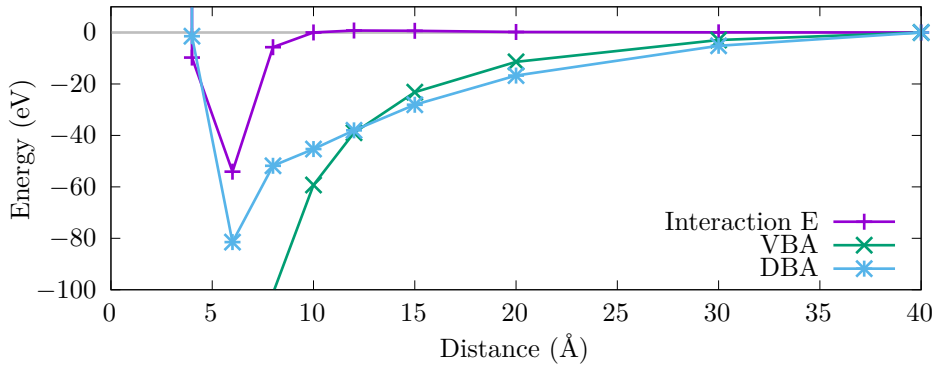

Figure 4.4: Favorable Interaction with water.

Isoleucine

...

Chapter 5

This is conclusion

...

Instructions by the Arenberg Doctoral School:

An extensive conclusion, including a global discussion of the research results, a discussion of the implications of the PhD research and future perspectives in regards to follow-up research.

Appendix A

This is myappendix

...

Instructions by the Arenberg Doctoral School:

Appendices: The appendices should include parts of the research which are essential for the work, but which may hamper the readability of the text, e.g. because of their length (mathematical deductions, experimental data, examples, figures, etc.).

Bibliography

[1] Jack Simons. Molecular anions. *The Journal of Physical Chemistry A*, 112(29):6401–6511, 2008.

[2] John M Herbert. The quantum chemistry of loosely-bound electrons. *Reviews in Computational Chemistry Volume 28*, pages 391–517, 2015.

[3] H Abdoul-Carime and C Desfrançois. Electrons weakly bound to molecules by dipolar, quadrupolar or polarization forces. *The European Physical Journal D-Atomic, Molecular, Optical and Plasma Physics*, 2:149–156, 1998.

[4] Jack Simons. Molecular anions perspective. *The Journal of Physical Chemistry A*, 127(18):3940–3957, 2023.

[5] Kenneth D Jordan and Feng Wang. Theory of dipole-bound anions. *Annual review of physical chemistry*, 54(1):367–396, 2003.

[6] Achintya Kumar Dutta, Turbasu Sengupta, Nayana Vaval, and Sourav Pal. Electron attachment to dna and rna nucleobases: An eomcc investigation. *International Journal of Quantum Chemistry*, 115(12):753–764, 2015.

[7] Enrico Fermi and Edward Teller. The capture of negative mesotrons in matter. *Physical Review*, 72(5):399, 1947.

[8] Thomas Sommerfeld. Coupling between dipole-bound and valence states: the nitromethane anion. *Physical Chemistry Chemical Physics*, 4(12):2511–2516, 2002.

[9] Do Hyung Kang and Sang Kyu Kim. Reaction dynamics of the nonvalence bound states of the anions. *Chemical Physics Reviews*, 5(4), 2024.

[10] Ryan C Fortenberry. Interstellar anions: the role of quantum chemistry. *The Journal of Physical Chemistry A*, 119(39):9941–9953, 2015.

[11] Jishnu Narayanan SJ, Divya Tripathi, Pooja Verma, Amitava Adhikary, and Achintya Kumar Dutta. Secondary electron attachment-induced radiation damage to genetic materials. *ACS omega*, 8(12):10669–10689, 2023.

[12] Barbora Sedmidubská and Jaroslav Kočišek. Interaction of low-energy electrons with radiosensitizers. *Physical Chemistry Chemical Physics*, 26(12):9112–9136, 2024.

[13] Connor J Clarke and Jan RR Verlet. Dynamics of anions: from bound to unbound states and everything in between. *Annual Review of Physical Chemistry*, 75, 2024.

[14] Stephen E Bradforth and Pavel Jungwirth. Excited states of iodide anions in water: A comparison of the electronic structure in clusters and in bulk solution. *The Journal of Physical Chemistry A*, 106(7):1286–1298, 2002.

[15] Piotr Skurski, Maciej Gutowski, and Jack Simons. How to choose a one-electron basis set to reliably describe a dipole-bound anion. *International Journal of Quantum Chemistry*, 80(4-5):1024–1038, 2000.

[16] Maciej Gutowski, Piotr Skurski, Alexander I Boldyrev, Jack Simons, and Kenneth D Jordan. Contribution of electron correlation to the stability of dipole-bound anionic states. *Physical Review A*, 54(3):1906, 1996.

[17] Guillaume Thiam and Franck Rabilloud. How accurately can dft describe non-valence anions? *Journal of Chemical Theory and Computation*, 19(10):2842–2849, 2023.

[18] Ove Christiansen, Henrik Koch, and Poul Jørgensen. The second-order approximate coupled cluster singles and doubles model cc2. *Chemical Physics Letters*, 243(5-6):409–418, 1995.

[19] Soumi Haldar and Achintya Kumar Dutta. A multilayer approach to the equation of motion coupled-cluster method for the electron affinity. *The Journal of Physical Chemistry A*, 124(19):3947–3962, 2020.

[20] AF Jalbout and L Adamowicz. Dipole-bound anions of adenine- water clusters. ab initio study. *The Journal of Physical Chemistry A*, 105(6):1033–1038, 2001.

[21] Connor J Clarke, E Michi Burrow, and Jan RR Verlet. The role of water molecules in the dissociation of an electron-molecule contact pair. *Nature Communications*, 16(1):2113, 2025.

[22] John M Herbert and Marc P Coons. The hydrated electron. *Annual review of physical chemistry*, 68(1):447–472, 2017.

[23] Iwona Anusiewicz, Piotr Skurski, and Jack Simons. Fate of dipole-bound anion states when hydrated. *The Journal of Physical Chemistry A*, 124(10):2064–2076, 2020.

[24] Maria Elena Castellani, Cate S Anstöter, and Jan RR Verlet. On the stability of a dipole-bound state in the presence of a molecule. *Physical Chemistry Chemical Physics*, 21(44):24286–24290, 2019.

[25] Jishnu Narayanan SJ, Pooja Verma, Amitava Adhikary, and Achintya Kumar Dutta. Electron attachment to the nucleobase uracil in diethylene glycol: The signature of a doorway. *ChemPhysChem*, 25(24):e202400581, 2024.

[26] Hsing-Yin Chen and Wen-Shyan Sheu. Precursors of the charge-transfer-to-solvent states in i-(h2o) n clusters. *Journal of the American Chemical Society*, 122(31):7534–7542, 2000.

[27] Jiande Gu, Jerzy Leszczynski, and Henry F Schaefer III. Interactions of electrons with bare and hydrated biomolecules: From nucleic acid bases to dna segments. *Chemical reviews*, 112(11):5603–5640, 2012.

[28] William James Russell. Address to the chemical section. *Chemical News and Journal of Physical Science*, 28:148–153, 1873.

[29] quinones. 2025.

[30] Lars Ernster and Gustav Dallner. Biochemical, physiological and medical aspects of ubiquinone function. *Biochimica et Biophysica Acta (BBA)-Molecular Basis of Disease*, 1271(1):195–204, 1995.

[31] Jiakuan Chen, Andrzej Pelc, João Ameixa, Fábris Kossoski, and Stephan Denifl. Low-energy electron interactions with methyl-p-benzoquinone: A study of negative ion formation. *ACS omega*, 9(36):38032–38043, 2024.

[32] J Ameixa, E Arthur-Baidoo, J Pereira-da Silva, M Ončák, JC Ruivo, MT do N Varella, F Ferreira Da Silva, and S Denifl. Parent anion radical formation in coenzyme q0: Breaking ubiquinone family rules. *Computational and Structural Biotechnology Journal*, 21:346–353, 2023.

[33] Stanislav A Pshenichnyuk, Alberto Modelli, Nail L Asfandiarov, and Alexey S Komolov. Ionizing radiation and natural constituents of living cells: low-energy electron interaction with coenzyme q analogs. *The Journal of chemical physics*, 153(11), 2020.

[34] Christopher W West, James N Bull, Erkki Antonkov, and Jan RR Verlet. Anion resonances of para-benzoquinone probed by frequency-resolved photoelectron imaging. *The Journal of Physical Chemistry A*, 118(48):11346–11354, 2014.

[35] James N Bull, Christopher W West, and Jan RR Verlet. Anion resonances and above-threshold dynamics of coenzyme q 0. *Physical Chemistry Chemical Physics*, 17(24):16125–16135, 2015.

[36] Marco Nonella. A quantum chemical investigation of structures, vibrational spectra and electron affinities of the radicals of quinone model compounds. *Photosynthesis research*, 55:253–259, 1998.

[37] Ana P Gamiz-Hernandez, Alexander Jussupow, Mikael P Johansson, and Ville RI Kaila. Terminal electron–proton transfer dynamics in the quinone reduction of respiratory complex i. *Journal of the American Chemical Society*, 139(45):16282–16288, 2017.

[38] Attila Szabo and Neil S Ostlund. *Modern quantum chemistry: introduction to advanced electronic structure theory*. Courier Corporation, 1996.

[39] Evgeny Epifanovsky, Andrew T. B. Gilbert, Xintian Feng, Joonho Lee, Yuezhi Mao, Narbe Mardirossian, Pavel Pokhilko, Alec F. White, Marc P. Coons, Adrian L. Dempwolff, Zhengting Gan, Diptarka Hait, Paul R. Horn, Leif D. Jacobson, Ilya Kaliman, Jörg Kussmann, Adrian W. Lange, Ka Un Lao, Daniel S. Levine, Jie Liu, Simon C. McKenzie, Adrian F. Morrison, Kaushik D. Nanda, Felix Plasser, Dirk R. Rehn, Marta L. Vidal, Zhi-Qiang You, Ying Zhu, Bushra Alam, Benjamin J. Albrecht, Abdulrahman Aldossary, Ethan Alguire, Josefine H. Andersen, Vishikh Athavale, Dennis Barton, Khadiza Begam, Andrew Behn, Nicole Bellonzi, Yves A. Bernard, Eric J. Berquist, Hugh G. A. Burton, Abel Carreras, Kevin Carter-Fenk, Romit Chakraborty, Alan D. Chien, Kristina D. Closser, Vale Cofer-Shabica, Saswata Dasgupta, Marc de Wergifosse, Jia Deng, Michael Diedenhofen, Hainam Do, Sebastian Ehlert, Po-Tung Fang, Shervin Fatehi, Qingguo Feng, Triet Friedhoff, James Gayvert, Qinghui Ge, Gergely Gidofalvi, Matthew Goldey, Joe Gomes, Cristina E. González-Espinoza, Sahil Gulania, Anastasia O. Gunina, Magnus W. D. Hanson-Heine, Phillip H. P. Harbach, Andreas Hauser, Michael F. Herbst, Mario Hernández Vera, Manuel Hodecker, Zachary C. Holden, Shannon Houck, Xunkun Huang, Kerwin Hui, Bang C. Huynh, Maxim Ivanov, Ádám Jász, Hyunjun Ji, Hanjie Jiang, Benjamin Kaduk, Sven Kähler, Kirill Khistyaev, Jaehoon Kim, Gergely Kis, Phil Klunzinger, Zsuzsanna Koczor-Benda, Joong Hoon Koh, Dimitri Kosenkov, Laura Koulias, Tim Kowalczyk, Caroline M. Krauter, Karl Kue, Alexander Kunitsa, Thomas Kus, István Ladjánszki, Arie Landau, Keith V. Lawler, Daniel Lefrancois, Susi Lehtola, Run R. Li, Yi-Pei Li, Jiashu Liang, Marcus Liebenthal, Hung-Hsuan Lin, You-Sheng Lin, Fenglai Liu, Kuan-Yu Liu, Matthias Loipersberger, Arne Luenser, Aaditya Manjanath, Prashant Manohar, Erum Mansoor, Sam F. Manzer, Shan-Ping Mao, Aleksandr V. Marenich, Thomas Markovich, Stephen Mason, Simon A. Maurer, Peter F.

McLaughlin, Maximilian F. S. J. Menger, Jan-Michael Mewes, Stefanie A. Mewes, Pierpaolo Morgante, J. Wayne Mullinax, Katherine J. Oosterbaan, Garrette Paran, Alexander C. Paul, Suranjan K. Paul, Fabijan Pavošević, Zheng Pei, Stefan Prager, Emil I. Proynov, Ádám Rák, Eloy Ramos-Cordoba, Bhaskar Rana, Alan E. Rask, Adam Rettig, Ryan M. Richard, Fazle Rob, Elliot Rossomme, Tarek Scheele, Maximilian Scheurer, Matthias Schneider, Nickolai Sergueev, Shaama M. Sharada, Wojciech Skomorowski, David W. Small, Christopher J. Stein, Yu-Chuan Su, Eric J. Sundstrom, Zhen Tao, Jonathan Thirman, Gábor J. Tornai, Takashi Tsuchimochi, Norm M. Tubman, Srimukh Prasad Veccham, Oleg Vydrov, Jan Wenzel, Jon Witte, Atsushi Yamada, Kun Yao, Sina Yeganeh, Shane R. Yost, Alexander Zech, Igor Ying Zhang, Xing Zhang, Yu Zhang, Dmitry Zuev, Alán Aspuru-Guzik, Alexis T. Bell, Nicholas A. Besley, Ksenia B. Bravaya, Bernard R. Brooks, David Casanova, Jeng-Da Chai, Sonia Coriani, Christopher J. Cramer, György Cserey, A. Eugene DePrince, Robert A. DiStasio, Andreas Dreuw, Barry D. Dunietz, Thomas R. Furlani, William A. Goddard, Sharon Hammes-Schiffer, Teresa Head-Gordon, Warren J. Hehre, Chao-Ping Hsu, Thomas-C. Jagau, Yousung Jung, Andreas Klamt, Jing Kong, Daniel S. Lambrecht, WanZhen Liang, Nicholas J. Mayhall, C. William McCurdy, Jeffrey B. Neaton, Christian Ochsenfeld, John A. Parkhill, Roberto Peverati, Vitaly A. Rassolov, Yihan Shao, Lyudmila V. Slipchenko, Tim Stauch, Ryan P. Steele, Joseph E. Subotnik, Alex J. W. Thom, Alexandre Tkatchenko, Donald G. Truhlar, Troy Van Voorhis, Tomasz A. Wesolowski, K. Birgitta Whaley, H. Lee Woodcock, Paul M. Zimmerman, Shirin Faraji, Peter M. W. Gill, Martin Head-Gordon, John M. Herbert, and Anna I. Krylov. Software for the frontiers of quantum chemistry: An overview of developments in the q-chem 5 package. *J. Chem. Phys.*, 155(8):084801, 2021.

[40] Christof Hättig and Florian Weigend. Cc2 excitation energy calculations on large molecules using the resolution of the identity approximation. *The Journal of Chemical Physics*, 113(13):5154–5161, 2000.

[41] Thom H Dunning Jr. Gaussian basis sets for use in correlated molecular calculations. i. the atoms boron through neon and hydrogen. *The Journal of chemical physics*, 90(2):1007–1023, 1989.

[42] Garrette Pauley Paran, Cansu Utku, and Thomas-Christian Jagau. On the performance of second-order approximate coupled-cluster singles and doubles methods for non-valence anions. *Physical Chemistry Chemical Physics*, 26(3):1809–1818, 2024.

[43] Jianmin Tao, John P Perdew, Viktor N Staroverov, and Gustavo E Scuseria. Climbing the density functional ladder: Nonempirical meta–generalized

gradient approximation designed for molecules and solids. *Physical review letters*, 91(14):146401, 2003.

[44] Stefan Grimme, Stephan Ehrlich, and Lars Goerigk. Effect of the damping function in dispersion corrected density functional theory. *Journal of computational chemistry*, 32(7):1456–1465, 2011.

[45] Jingjing Zheng, Xuefei Xu, and Donald G Truhlar. Minimally augmented karlsruhe basis sets. *Theoretical Chemistry Accounts*, 128:295–305, 2011.

[46] Florian Weigend and Reinhart Ahlrichs. Balanced basis sets of split valence, triple zeta valence and quadruple zeta valence quality for h to rn: Design and assessment of accuracy. *Physical Chemistry Chemical Physics*, 7(18):3297–3305, 2005.

[47] Christine E Schulz, Achintya Kumar Dutta, Róbert Izsák, and Dimitrios A Pantazis. Systematic high-accuracy prediction of electron affinities for biological quinones. *Journal of Computational Chemistry*, 39(29):2439–2451, 2018.

[48] Schrödinger, LLC. The PyMOL molecular graphics system. 2015.

[49] Samer Gozem and Anna I Krylov. The ezspectra suite: An easy-to-use toolkit for spectroscopy modeling. *Wiley Interdisciplinary Reviews: Computational Molecular Science*, 12(2):e1546, 2022.

[50] Samer Gozem and Anna I Krylov. Photoionization and photodetachment spectra from equation-of-motion coupled-cluster dyson orbitals. *Chem. Lett*, 6:4532–4540, 2015.

Statement on the use of Generative AI

Instructions by the Arenberg Doctoral School:

Read the guidelines in relation to GenAI at KU Leuven and add the ‘statement on the use of Generative AI’ in your manuscript.

Generative AI was used for lenguage and coding assistance (ChatGPT, MicrosoftCopilot, LeChat).
The text, code, and images in this thesis are my own (unless otherwise specified). Generative AI has only been used in accordance with the KU Leuven guidelines and appropriate references have been added. I have reviewed and edited the content as needed and I take full responsibility for the content of the thesis.

DEPARTMENT OF CHEMISTRY
DEPARTMENT OF CHEMISTRY
Celestijnenlaan 200A box 2402
B-3001 Leuven
first.name@dept.kuleuven.be
https://chem.kuleuven.be/en/research/qcpc/tue/